Asian Journal of Chemical Sciences

2(1): 1-20, 2017; Article no.AJOCS.31015

The Numerical Study of Effects of Soret, Dufour and Viscous Dissipation Parameters on Steady MHD Casson Fluid Flow through non-Darcy Porous Media

Bhim Sen Kala[1*]

[1]Koneru Lakshmaiah University, Guntur, 522502, A. P., India.

Author's contribution

The sole author designed, analyzed and interpreted and prepared the manuscript.

Article Information

DOI: 10.9734/AJOCS/2017/31015
Editor(s):
(1) Dimitrios P. Nikolelis , Chemistry Department, Athens University, Panepistimiopolis-Kouponia, Athens, Greece.
Reviewers:
(1) K. Gangadhar, Acharya Nagarjuna University Ongole Campus, India.
(2) Sami Ullah Khan, International Islamic University Islamabad 44000, Pakistan.
(3) R. Srinivasa Raju, GITAM University, Telangana State, India.
(4) A. Mahdy, South Valley University, Qena, Egypt.
(5) V. Ramachandra Prasad, Madanapalle Institute of Technology and Science, Madanapalle, India.
(6) T.S. L Radhika, BITS Pilani-Hyderabad Campus, Hyderabad, India.
Complete Peer review History: http://prh.sdiarticle3.com/review-history/17761

Original Research Article

Received 14th December 2016
Accepted 21st January 2017
Published 8th February 2017

ABSTRACT

In the present paper the numerical study of effects of Soret, Dufour and viscous dissipation parameters on steady MHD Casson fluid flow through non-Darcy porous medium is explored. By suitable similarity transformations, the governing boundary layer equations are transformed to ordinary differential equations. The method, the numerical computation with bvp4c, a MATLAB program, is applied to solve these equations. The effects of magnetic parameter, Soret parameter, Dufour parameter, Prandtl number, Schmidth number, Eckert number, and Casson parameter on velocity, heat transfer, and concentration profiles, Skin- friction, local Nusselt number and local Sherwood number are computed and discussed numerically and presented through tables and graphs.

Keywords: Magnetohydrodynamics; Casson fluid; magnetic parameter; Soret number; Dufour number.

**Corresponding author: E-mail: bhimskala@gmail.com;*

NOMENCLATURE AND SI UNITS

μ : Dynamic viscosity ($kgm^{-2}s^{-1}$)
υ : Kinematic viscosity ($m^{-2}s^{-1}$)
B : Magnetic field(N/(mA))
H : Convective heat transfer coefficient (W/m^2K)
c : Specific heat (J/kgK)
D : Mass diffusivity(m^2s^{-1})
G : Acceleration due to gravity (ms^{-2})
K : Thermal conductivity($Wm^{-1} K^{-1}$)
M : Mass kg
V : Volume m^3
ρ : Density kg/m^3
t : Time(s)
u : Horizontal component of velocity(m/s)
v : Vertical component of velocity(m/s)
T : Temperature of fluid (K)
β : Thermal expansion coefficient(K^{-1})
M : Magnetic parameter
N : Stretching index parameter
Nu : Local Nusselt number
Pr : Prandtl number Prandtl number
Re : Local Reynold number
Sc : Smidth number
Sh : Local Sherwood number
C : Concentration of fluid
Gr_T : Thermal Grashof number
C_p : Specific heat at constant pressure
Gr_c : Mass(concentration) Grashof number
X : Distance along the plate distance along the plate
α : Thermal diffusivity
η : Similarity variable
x, y : Cartesian coordianates
θ : Dimensionless temperature
ψ : Dimentiosless stream function

1. INTRODUCTION

Many natural, industrial as well as biological fluids (such as mud, condensed milk, glues, lubricating greases, paints, sugar solution, shampoos and tomato paste, polymers, liquid detergents, blood, fruit juices etc.) change their viscosity or flow behaviour under stress; and thus deviate from the classical Newton's law of viscosity. Different models of non-Newtonian fluids based on their diverse flow behaviours have been proposed by the researchers.

The rheological model was introduced originally by Casson [1] in his research on a flow equation for pigment oil-suspension of printing ink. Bird et al. [2] investigated the rheology and flow of visco-plastic materials. He reported that Casson model constitutes a plastic fluid model which exhibits shear thinning characteristics, yield stress, and high shear viscosity. Casson fluid behaves as solid when the shear stress is less than the yield stress and it starts to deform when shear stress becomes greater than the yield stress.

The fundamental analysis of the flow field of non-Newtonian fluids in a boundary layer adjacent to a stretching sheet or an extended surface is very important and is an essential part in the study of fluid dynamics, and heat and mass transfer.

Sakiadis [3] studied boundary layer behaviour on continuous solid surfaces: II. The boundary layer on continuous flat surface. Crane [4] studied the flow past a stretching plane. Nield et al. [5] studied convection in porous media.

Mukhopadhyay [6] investigated Casson fluid flow and heat transfer over a nonlinearly stretching surface. Mustafa et al. [7] studied Model for the flow of Casson nanofluid past a non-linearly stretching sheet, considering magnetic field effects. Medikare et al. [8] studied MHD stagnation point flow of a Casson fluid over a nonlinearly stretching sheet with viscous dissipation.

Pramanik [9] studied Casson fluid flow and heat transfer past an exponentially porous stretching surface in presence of thermal radiation. Raju et al. [10] studied heat and mass transfer in magnetohydrodynamic Casson fluid over an exponentially permeable stretching surface. Saidulu et al. [11] studied slip effects on MHD flow of Casson fluid over an exponentially stretching sheet in presence of thermal radiation, heat source/sink and chemical reaction.

Sharada et al. [12] studied MHD mixed convection flow of a Casson fluid over an exponentially stretching surface with the effects of Soret, Dufour, thermal radiation and chemical reaction. Mukhopadhyay et al [13] studied exact solutions for the flow of Casson fluid over a stretching surface with transpiration and heat transfer effects. Hayat et al. [14] investigated Soret and Dufour effects on magnetohydrodynamic (MHD) flow of Casson fluid.

Mahdy [15] studied heat transfer and flow of a Casson fluid due to a stretching cylinder with the Soret and Dufour effects. Animasaun [16] studied effects of thermophoresis, variable viscosity and thermal conductivity on free convective heat and mass transfer of non-Darcian MHD dissipative Casson fluid flow with suction and nth order of chemical reaction.

Ullah et al. [17] investigated Effects of slip condition and Newtonian heating on MHD flow of Casson fluid over a nonlinearly stretching sheet saturated in a porous medium.

Some recent studies concerning the flow, heat and mass transfer analysis of Casson fluid can be found in Refs [18–58].

We consider (1) non-Darcy porous medium, (2) thermo –diffusion(Dufour term) term in energy equation, (3) mass equations, (4) diffusion - thermo term (Soret term) in the mass equation and (5) nonlinear surface (6), velocity slip factor, thermal slip factor, and mass slip factor in boundary conditions of velocity, temperature, and concentration respectively. In the study of references as mentioned above, these terms, simultaneously in one problem, are not investigated with the flow over nonlinear surface.

The present work is the extension of Ullah et al. [17] work, by considering above terms.

It deals with the numerical study of effects of Soret Dufour and viscous dissipation parameters on steady MHD Casson fluid flow through non-Darcy porous medium.

2. MATHEMATICAL FORMULATION OF THE PROBLEM

In the formulation of the problem we consider following assumptions. Casson fluid is incompressible and electrically conducting. Flow is steady, laminar and two dimensional over a nonlinearly stretching sheet. Flow region is in non-Darcy porous medium. It is under the influence of transverse magnetic field B .The sheet is stretched nonlinearly along the x-axis (i.e. y=0) with velocity $u_w(x) = c\,x^n$;origin is taken as fixed and the fluid flow is confined to y>0. Here c is constant and $n(n \ge 0)$ is the nonlinear stretching sheet parameter; $n=1$ represents the linear sheet case and $n \ne 1$ is for nonlinear case. The magnetic Reynolds number of the flow is taken to be small enough so that induced magnetic field is assumed to be negligible in comparison with applied magnetic field so that $B=(0, B(x), 0)$, where $B(x)$ is the applied magnetic field acting normal to the plate and varies in strength as a function of x. The flow is assumed to be in the x-direction which is taken along the plate and y-axis is normal to it. There is a constant suction/injection velocity v_w normal to the plate.

Under these assumptions the rheological equation for incompressible flow of Casson fluid is given by (Sharada et al. [12], Mukhopadhyay et al. [13])

$$\tau_{ij} = \begin{cases} 2(\mu_B + p_y/\sqrt{2\pi})e_{ij} & \pi > \pi_c \,, \\ 2(\mu_B + p_y/\sqrt{2\pi_c})e_{ij} & \pi < \pi_c \end{cases}.$$

where $\pi = e_{ij}\,e_{ij}$ and e_{ij} is the $(i,j)-\mathrm{th}$ component of the deformation rate , π is the product of the components of deformation , π_c is critical value of the product based on the non-Newtonian model, μ_B is the plastic dynamic viscosity of the non-Newtonian fluid, and p_y is the yield stress of the fluid. The viscosity and thermal conductivity of the fluid are assumed to be constant. There is thermo-diffusion effect as well as diffusion-thermo effect. The pressure gradient, body forces and Joule heating are neglected compared with the effect of viscous dissipation. The temperature and concentration of the stretching surface are always greater than their free stream values. The flow configuration and the coordinate system are shown in Fig. 1.

Under the above assumptions and using Boussinesq approximation, boundary layer equations for flow with heat and mass transfer in Casson fluid are given by the following.

The continuity equation:

$$\frac{\partial u}{\partial x} + \frac{\partial v}{\partial y} = 0\,, \tag{1}$$

The momentum equation:

$$u\frac{\partial u}{\partial x} + v\frac{\partial u}{\partial y} = \upsilon\left(1+\frac{1}{\beta}\right)\frac{\partial^2 u}{\partial y^2} + g\beta_T(T - T_\infty) + g\beta_C(C - C_\infty) - \frac{\sigma B^2(x)}{\rho}u - \frac{\upsilon}{K}u - \frac{b}{\sqrt{K}}u^2 \tag{2}$$

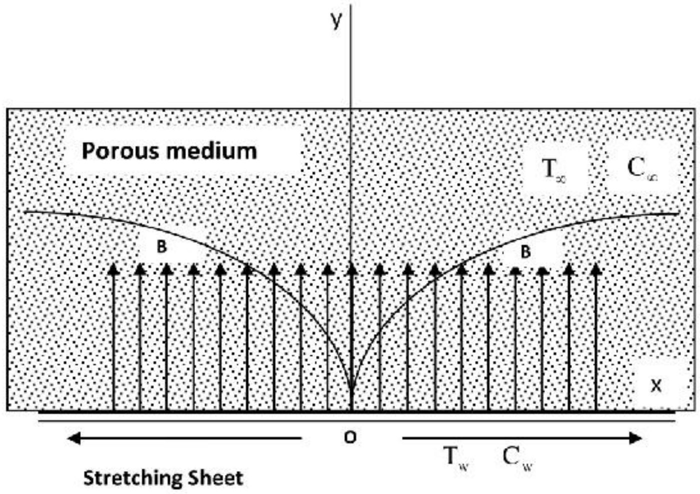

Fig. 1. Physical model and coordinate system

The energy equation:

$$u\frac{\partial T}{\partial x}+v\frac{\partial T}{\partial y}$$
$$=\alpha\frac{\partial^2 T}{\partial y^2}+\left(\frac{D_m K_T}{C_S C_P}\right)\frac{\partial^2 C}{\partial y^2}+\frac{\mu}{\rho\, C_p}\left(1+\frac{1}{\beta}\right)\left(\frac{\partial u}{\partial y}\right)^2 \quad (3)$$

The mass equation:

$$u\frac{\partial C}{\partial x}+v\frac{\partial C}{\partial y}=D_m\frac{\partial^2 C}{\partial y^2}+\left(\frac{D_m K_T}{T_M}\right)\frac{\partial^2 T}{\partial y^2} \quad (4)$$

where u and v are velocity components along x and y axes, respectively, ρ is fluid density, υ is kinematic viscosity, μ is dynamic viscosity, $\beta=\mu_B\sqrt{2\pi}/p_y$ is the Casson fluid parameter, σ is the electrical conductivity of the fluid and is assumed to be constant, β_T is the coefficient of thermal expansion, β_C is the coefficient of concentration expansion, T_W is the temperature of the fluid at the stretching sheet, T is the temperature of the fluid within the boundary layer, T_∞ is the temperature of the fluid outside the boundary layer, k is the thermal conductivity of the fluid, C_P is the specific heat at constant pressure p, C_W is the concentration of the fluid at the stretching sheet, C is the concentration of the fluid within the boundary layer, C_∞ is the concentration of the fluid outside the boundary layer, D_M is the chemical molecular diffusivity. Here, g is the acceleration due to gravity. The applied magnetic field is $B = B_0\, x^{\frac{n-1}{2}}$, where B_0 is assumed to be constant.

Boundary conditions (Ullah et al. [17]):

$$\begin{aligned}&At\;\; y=0: u=cx^n+N_1\upsilon\left(1+\frac{1}{\beta}\right)\frac{\partial u}{\partial y},\quad v=0,\;\; \frac{\partial T}{\partial y}=-h_s(T-T_w),\, \frac{\partial C}{\partial y}=-h_c(C-C_w)\\ &As\;\; y\to\infty: u\to 0,\; T\to T_\infty\,, C\to C_\infty .\end{aligned} \quad (5)$$

Here $N_1(x) = N\, x^{-\frac{n-1}{2}}$ denotes velocity of slip factor; it depends upon x, and $h_s(x)=h_{T0}\,c\,x^{\frac{n-1}{2}}$ represents the heat transfer parameter for Newtonian heating or temperature slip factor, and $h_c(x)=h_{c0}\,c\,x^{\frac{n-1}{2}}$ is concentration slip factor.

We consider following dimensionless variable to transform the system of equations (2), (3), (4) and (5) into a dimensionless form (Ullah et al. [17]):

$$\psi = \left(\frac{2\nu c}{n+1}\right)^{\frac{1}{2}} x^{\frac{n+1}{2}} f(\eta),\ \eta = \left(\frac{c(n+1)}{2\nu}\right)^{\frac{1}{2}} x^{\frac{n-1}{2}} y,\ \theta(\eta) = \frac{(T-T_\infty)}{(T_w - T_\infty)},\ \phi(\eta) = \frac{(C-C_\infty)}{(C_w - C_\infty)},$$
$$u = \frac{\partial \psi}{\partial y}, v = -\frac{\partial \psi}{\partial x},\ u = cx^n\ f'(\eta),\ v = -\left(\frac{c\upsilon(n+1)}{2}\right)^{\frac{1}{2}} x^{\frac{n+1}{2}} \left(f(\eta) + \frac{n-1}{n+1}\eta f'(\eta)\right) \tag{6}$$

Here η is the similarity variable. ψ is stream function. $c\,(c>0)$ is a parameter related to the surface stretching speed, n is the power index related to the surface stretching speed.

Introducing these variables in the equations we get the following dimensionless forms of the equations:

$$(1+\frac{1}{\beta})f''' + f f'' + \frac{2n}{n+1} f'^2 + d_1\theta + d_2\phi - (M + (1/K_1))f' - Fs\left(f'\right)^2 = 0\,, \tag{7}$$

$$\frac{1}{\Pr}\theta'' + f\theta' + \left(1+\frac{1}{\beta}\right) Ec\, f''^2 = 0\ , \tag{8}$$

$$\frac{1}{Sc}\phi'' + f\phi' + Sr\,\theta'' = 0\,, \tag{9}$$

with parameters:

$$\left.\begin{aligned}
&M = \frac{2\sigma B_0^2}{\rho c}, K1 = \frac{Kcx^{n-1}}{2\nu}, Fs = \frac{2bx}{\sqrt{K}}, \Pr = \frac{\upsilon}{\alpha} = \frac{\rho\upsilon C_p}{k} = \frac{\mu C_p}{k},\\
&Gr_T = \frac{2g\beta_T(T_w - T_\infty)}{(n+1)c^2 x^{2n-1}},\ Gr_C = \frac{2g\beta_C(C_w - C_\infty)}{(n+1)c^2 x^{2n-1}}, u = cx^n\\
&Ec = \frac{u^2}{C_p(T_w - T_\infty)} = \frac{c^2 x^{2n}}{C_p(T_w - T_\infty)}\,'\nu = \frac{\mu}{\rho},\\
&Sc = \frac{\upsilon}{D_m}, Du = \frac{D_m\ K_T\ (C_W - C_\infty)}{\upsilon C_S C_P (T_W - T_\infty)}, Sr = \frac{D_m\ K_T\ (T_W - T_\infty)}{\upsilon T_\infty (C_W - C_\infty)}.
\end{aligned}\right\} \tag{10}$$

Here M is magnetic parameter(Hartmann number); K1 is Permeability parameter; Fs is Forchheimer parameter; Pr is Prandtl number; Gr_T is thermal Grashof number; Gr_C is concentration Grashof number; Ec is Eckert number; Du is Dufour number; Sc is Schmidt number ;and Sr is Soret number. And corresponding boundary conditions are as follow:

$$f(0) = 0, f'(0) = 1 + \delta\left(1+\frac{1}{\beta}\right)f''(0), \theta'(0) = -\gamma_1[1+\theta(0)], \phi'(0) = -\gamma_2[1+\phi(0)]$$
$$f'(\infty) = 0,\ \theta(\infty) = 0, \phi(\infty) = 0 \tag{11}$$

Where

$$N = N_1\, x^{-\frac{n-1}{2}}, \delta = N\left(\frac{(n+1)\,c\,\upsilon}{2}\right)^{\frac{1}{2}},\; h_T = h_{T0}\, c\; x^{\frac{n-1}{2}}, \gamma_1 = h_{T0}\left(\frac{2\,\upsilon}{c\,(n+1)}\right)^{\frac{1}{2}}$$
$$h_C = h_{C0}\, c\; x^{\frac{n-1}{2}}, \gamma_1 = h_{C0}\left(\frac{2\,\upsilon}{c\,(n+1)}\right)^{\frac{1}{2}} \tag{12}$$

δ is called velocity slip parameter, γ_1 is called thermal slip parameter, and γ_2 is called concentration slip parameter.

The physical quantities of Engineering interest are the Skin-friction coefficient (rate of shear stress), the couple stress coefficient at the sheet, the local Nusselt number (rate of heat transfer), and the local Sherwood number (rate of mass transfer).

The local Skin-friction C_f, local Nusselt Number Nu_x and local Sherwood Number Sh_x are defined as follow:

$$\left.\begin{aligned} C_f &= \frac{\tau_w}{\frac{\rho U_w^2}{2}} = \frac{\mu_B\left(1+\frac{1}{\beta}\right)\left(\frac{\partial u}{\partial y}\right)_{y=0}}{\frac{\rho U_w^2}{2}} \Rightarrow C_f = \left(\frac{2\nu(n+1)}{c}\right)^{\frac{1}{2}} x^{-\frac{(n+1)}{2}} f''(0),\\ C_f &= \left(\frac{2(n+1)}{\mathrm{Re}}\right)^{\frac{1}{2}}\left(1+\frac{1}{\beta}\right) f''(0),\;\; \mathrm{Re} = \frac{cx^{(n+1)}}{\nu}. \end{aligned}\right\} \tag{13}$$

$$\left.\begin{aligned} Nu &= -\frac{x\left(\frac{\partial T}{\partial y}\right)_{y=0}}{T_w - T_\infty} = -\left(\frac{c(n+1)}{2\nu}\right)^{\frac{1}{2}} x^{\frac{(n+1)}{2}}\theta'(0),\\ Nu &= -\left(\frac{(n+1)cx^{(n+1)}}{2\nu}\right)^{\frac{1}{2}}\theta'(0) = -\left(\frac{(n+1)}{2}\mathrm{Re}\right)^{\frac{1}{2}}\theta'(0). \end{aligned}\right\} \tag{14}$$

Here $-\left(\frac{\partial T}{\partial y}\right)_{y=0}$ is a heat flux from the surface of the sheet.

$$\left.\begin{aligned} Sh &= -\frac{x\left(\frac{\partial C}{\partial y}\right)_{y=0}}{C_w - C_\infty} = -\left(\frac{c(n+1)}{2\nu}\right)^{\frac{1}{2}} x^{\frac{(n+1)}{2}}\phi'(0),\\ Sh &= -\left(\frac{(n+1)cx^{(n+1)}}{2\nu}\right)^{\frac{1}{2}}\phi'(0) = -\left(\frac{(n+1)}{2}\mathrm{Re}\right)^{\frac{1}{2}}\phi'(0). \end{aligned}\right\} \tag{15}$$

Here $-\left(\frac{\partial C}{\partial y}\right)_{y=0}$ is a mass flow rate from the surface of the sheet and Re is the local Reynold Number.

3. METHOD OF NUMERICAL SOLUTION

The numerical solutions are obtained using the equations (7)-(9) and boundary conditions (11) for some values of the governing parameters, namely, the magnetic parameter M, Soret number Sr ,Dufour number Du, Casson fluid parameter β , Prandtl number Pr, Schmidth number Sc, Eckert number Ec . Effects of M, Sr, Du, β, Pr, Sc, Ec on the steady boundary layer flow are discussed in detail. The numerical computation is done using the MATLAB in-built numerical solver bvp4c. In the computation we have taken $\eta_\infty = 10$ and axis according to the clear figure-visuality.

4. RESULT ANALYSIS AND DISCUSSION

In order to analyze the behaviour of non-dimensional linear velocity $f'(\eta)$, temperature $\theta(\eta)$, and concentration $\phi(\eta)$ profiles of the physical problem, numerical calculations are carried out for various values of magnetic parameter M, Soret number Sr ,Dufour number Du, Casson fluid parameter β, Prandtl number Pr, Schmidth number Sc,and Eckert number Ec . Also, the Skin-friction factor and local Nusselt and local Sherwood numbers are discussed. For illustration of the results, the numerical data are tabulated in Tables 1-8 and plotted in Figs. 2–26.

For the convenience in calculation in Matlab following symbles are used for respective symbols used in modelling equations and boundary conditions:

$$a1 = f''(0),\ a2 = \theta'(0),\ a3 = \phi'(0),\ d = \delta,\ d1 = Gr_T,\ d2 = Gr_C,\ b = \beta,\ m1 = \gamma_1,\ m2 = \gamma_2,\ n1 = n.$$

The results for Skin-friction and local Nusselt number are compared with the previous published results, and are shown in Tables 1–2. It is observed that the obtained results are in good agreement with the published results.

Tables 1 and 2 present the values of Skin-friction coefficient and local Nusselt number for different values of nonlinear stretching parameter n1 and Prandtl number Pr, respectively. The present results are compared with the results of Cortell [18] and Ullah et al. [17]. It is also observed from Table 1 that magnitude of Skin-friction coefficient $\left|\left(1+\frac{1}{\beta}\right)f''(0)\right|$, increases with the increase in n1 whereas local Nusselt number decreases with the increase in n1 and increases with increase in Pr (Table 2).

Figs. 2–26 are plotted to study the effects of various parameters (b, n1, M, Da, Fs, d , d1, d2, m1, m2, a1, a2, a3, Pr, Sc, Ec, Du and Sr) on the dimensionless velocity, temperature and concentration profiles.

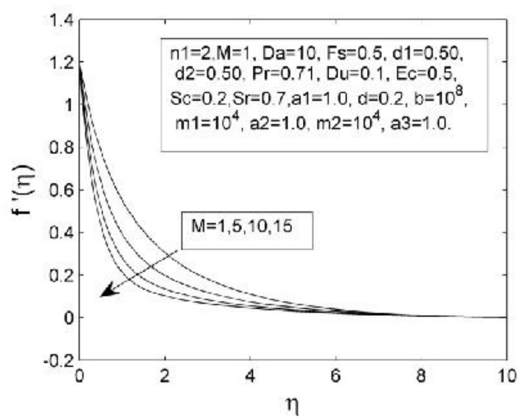

Fig. 2. Velocity profile $f'(\eta)$ with respect to similarity transformation η for some values of Magnetic parameter M

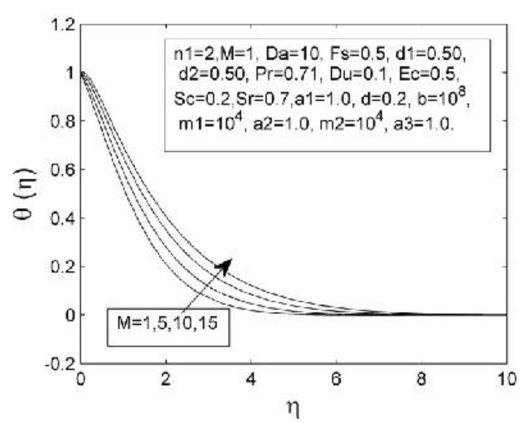

Fig. 3. Temperature profile $\theta(\eta)$ with respect to similarity transformation η for some values of Magnetic parameter M

The effect of M is illustrated in Fig. 2. All the trajectories are of same family with the magnetic number in between 1 and 15. It is seen that fluid velocity reduces as M increases. It is due to the fact that drag force, also known as Lorentz force is produced when magnetic field is applied to the fluid. This force has the tendency to slow down the velocity of the fluid in the boundary layer region. The decreasing pattern of velocity field with the increase in similarity variable shows that transverse magnetic field opposes the transport phenomenon. Thus the momentum boundary layer thickness decreases as M increases.

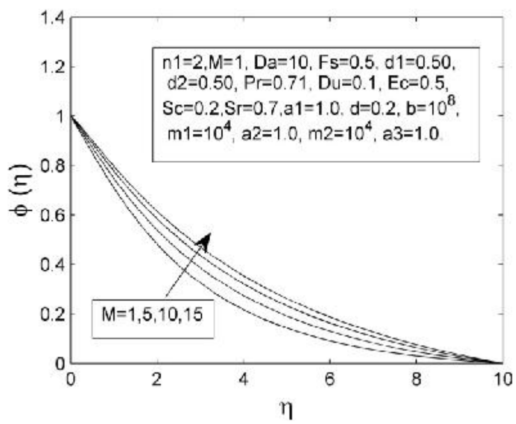

Fig. 4. Concentration profile $\phi(\eta)$ with respect to similarity transformation η for some values of Magnetic parameter M

Fig. 3 shows the behaviour of temperature profile for increasing values of Magnetic parameter M. The increasing values of M increase the fluid temperature as well as thermal boundary layer thickness. It is also observed that higher values of M increase the fluid temperature significantly and boundary layer expands away from the wall. The explanation of this phenomenon is that the increasing M leads to a increase in thermal diffusion and results in thickening of boundary layer region.

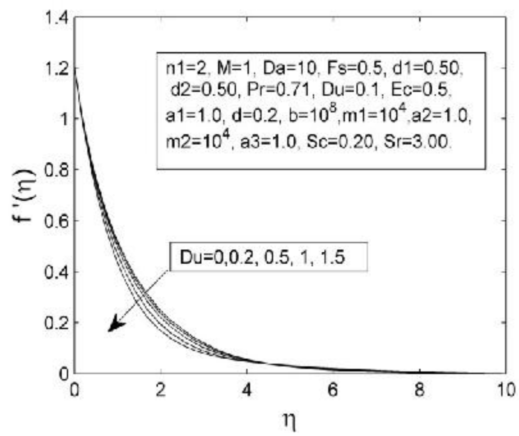

Fig. 5. Velocity profile $f'(\eta)$ with respect to similarity transformation η for some values of Dufour parameter Du

Fig. 4 shows the behaviour of concentration profile for increasing values of Magnetic parameter M. The increasing values of M increase the fluid concentration as well as concentration boundary layer thickness. It is also observed that higher values of M increase the fluid concentration significantly and boundary layer expands away from the wall. The explanation of this phenomenon is that the increasing M leads to a increase in concentration diffusion and results in thickening boundary layer. Thus, the increasing values of M increase the fluid concentration as well as concentration boundary layer thickness.

Table 1. Comparison of $-f''(0)$ for different values of n1 with Fs=0.0, d1=0.0, d2=0.0, d=0.0, m1=10^4, m2=10^4, M=0, Pr=1.00, Du=0.0, Sc=0.22, a1=0.0, a2=1.0, a3=1.0, b=10^8, Ec=0.0, Da=10^7, Sr=0

	$-f''(0)$		
n1	**Cortell [18]**	**Ullah et al. [17]**	**Present**
0.0	0.627547	0.6276	0.627631963479766
0.2	0.766758	0.7668	0.766906263551595
0.5	0.889477	0.8896	0.889594172073448
1	1.0	1.0	1.000062567556568
3	1.148588	1.1486	1.148660394543063
10	1.234875	1.2349	1.234952969673218
100	1.276768	1.2768	1.276830449563257

Table 2. Comparison of local Nusselt number $-\theta'(0)$ for various values of Pr and n1 with Fs=0.0, d1=0.0, d2=0.0, d=0.0, m1=10^4, m2=10^4, M=0, Pr=1.00, Du=0.0, Sc=0.22, a1=0.0, a2=1.0, a3=1.0, b=10^8, Ec=0.0, Da=10^7, Sr=0

	$-\theta'(0)$,Pr=1,		
n1	Cortell [18]	Ullah et al. [17]	Present
0.2	0.610262	0.6102	0.610277445039946
0.5	0.595277	0.5949	0.595283487517005
1.5	0.574537	0.5747	0.574829838650739
3.0	0.564472	0.5647	0.564775152915357

The effect of Dufour parameter is illustrated in Fig. 5. It is seen that fluid velocity profile reduces as Du increases and causes thinning of the corresponding boundary layer.

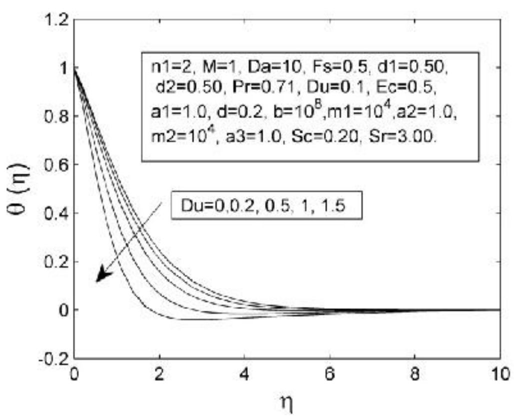

Fig. 6. Temperature profile $\theta(\eta)$ with respect to similarity transformation η for some values of Dufour parameter Du

It is shown in Fig. 6 that the temperature profile decreases with the increase i Dufour parameter and causes thinning of the corresponding boundary layer.

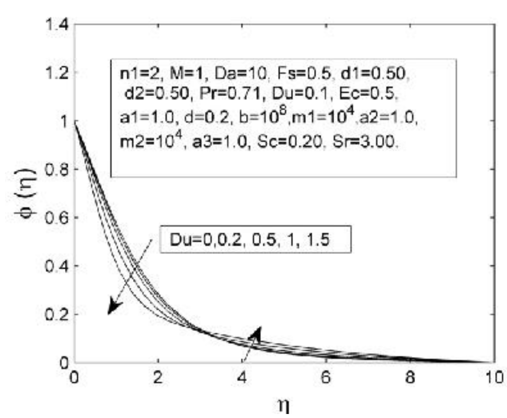

Fig. 7. Concentration profile $\phi(\eta)$ with respect to similarity transformation η for some values of Dufour parameter Du

It is shown in Fig. 7 that with the variation in the value of Dufour number Du, the concentration profiles show presence of point of intersection at some value of similarity variable in its (similarity variable's) range. Before the point of intersection concentration profiles decrease and after the point of intersection concentration profiles increase with the increase in Du and thus causes thinning before the point of intersection and thickening after the point of intersection of the corresponding boundary layers.

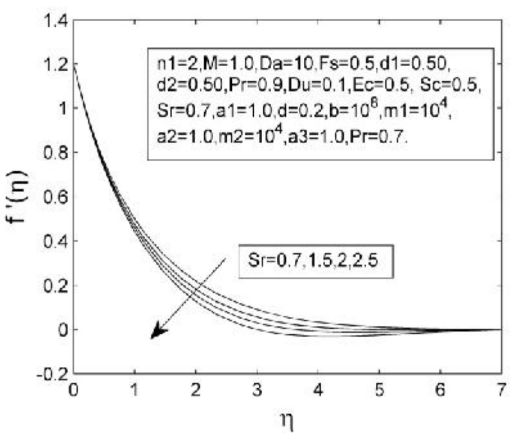

Fig. 8. Velocity profile $f'(\eta)$ with respect to similarity transformation η for some values of Soret parameter Sr

It is seen in Fig. 8 that velocity profile decreases with increasing Soret number and causes thinning of the corresponding boundary layer.

It is seen in Fig. 9 that the temperature profile increases with increasing Soret number and causes thickening of the corresponding boundary layer.

It is seen in Fig. 10 that the concentration profile decreases with increasing Soret number and causes thinning of the corresponding boundary layer.

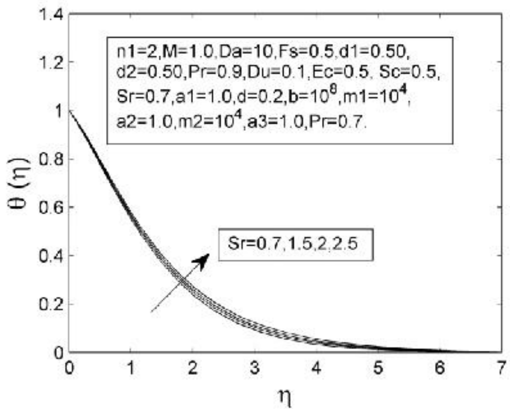

Fig. 9. Temperature profile $\theta(\eta)$ with respect to similarity transformation η for some values of Soret parameter Sr

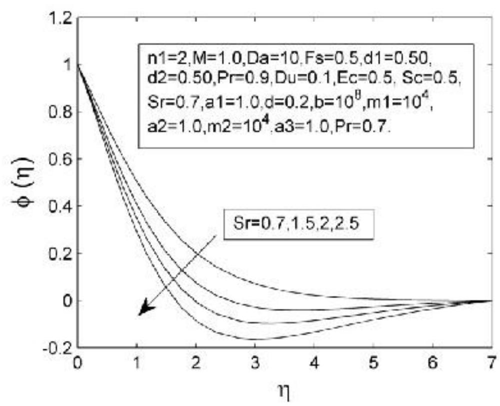

Fig. 10. Concentration profile $\phi(\eta)$ with respect to similarity transformation η for some values of Soret parameter Sr

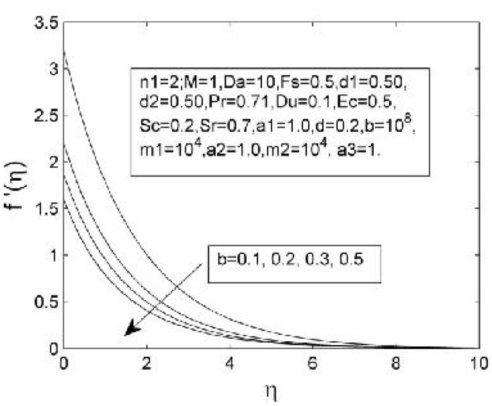

Fig. 11. Velocity profile $f'(\eta)$ with respect to similarity transformation η for some values of Casson parameter b

It is observed from Fig. 11 above that velocity profile decreases with the increase in Casson parameter b. physically, with increase in b, the fluid becomes more viscous and in result the fluid velocity reduces. Also, the momentum boundary layer thickness decreases as b increases. Further, as $b \to \infty$ the present phenomenon reduces to Newtonian fluid.

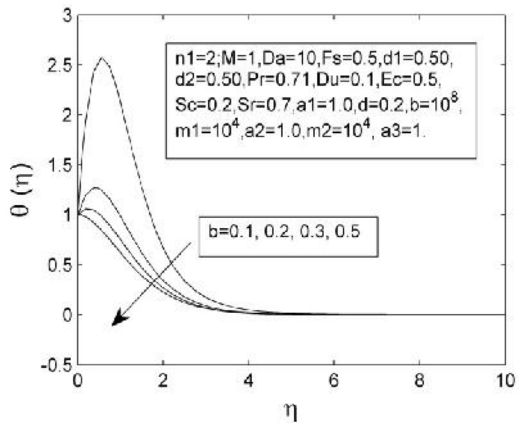

Fig. 12. Temperature profile $\theta(\eta)$ with respect to similarity transformation η for some values of Casson parameter b

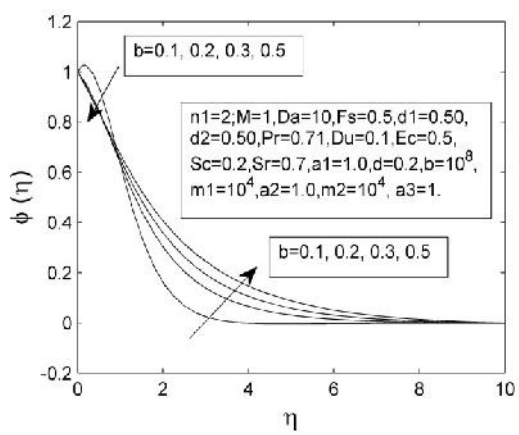

Fig. 13. Concentration profile $\phi(\eta)$ with respect to similarity transformation η for some values of Casson parameter b

It is observed from Fig. 12 that with the increase in the value of Casson parameter b, temperature profiles decrease. Also each curve shows having maxima and point of inflexion at some points in the range of similarity variable. And it causes thinning of the corresponding boundary layer before the point of inflexion.

It is observed from Fig. 13 that with the variation in the value of Casson parameter b, the concentration profiles shows presence of point of inflexion at some values of the similarity variable in its (similarity variable's) range. Before the point of inflexion concentration profile decreases and after the point of inflexion concentration profile increases with the increase in Casson parameter and thus causes thinning before the point of inflexion and thickening after the point of inflexion of the corresponding boundary layer.

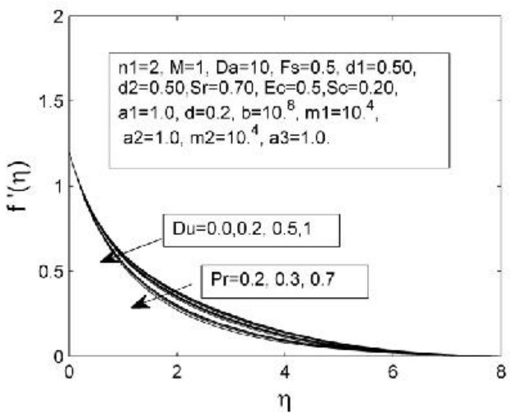

Fig. 14. Velocity profile $f'(\eta)$ with respect to similarity transformation η for some values of Dufour parameter Du and Prandtl number Pr

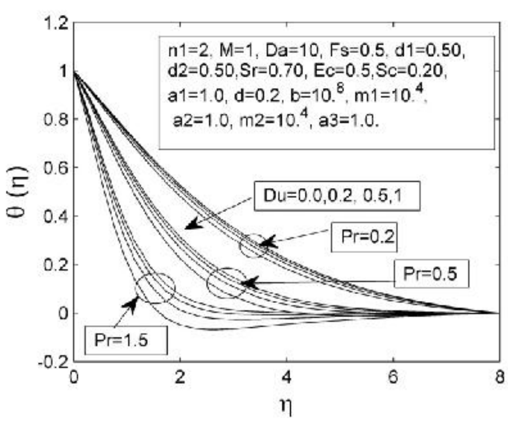

Fig. 15. Temperature profile $\theta(\eta)$ with respect to similarity transformation η for some values of Dufour parameter Du and Prandtl number Pr

It is observed from Fig. 14 that velocity profiles decrease with the increase in Dufour parameter Du and Prandtl number Pr and thus cause thinning of the corresponding boundary layers.

It is observed from Fig. 15 that temperature profiles decrease with the increase in Dufour parameter Du and Prandtl number Pr and thus cause thinning of the corresponding boundary layers.

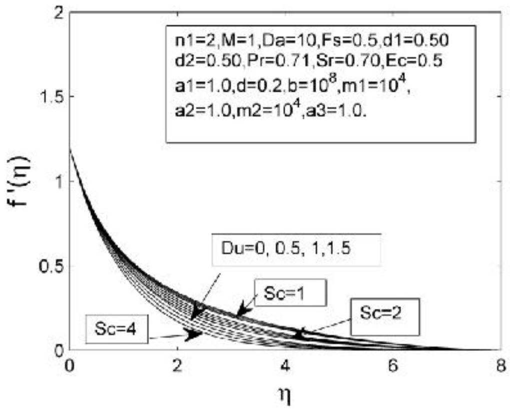

Fig. 16. Velocity profile $f'(\eta)$ with respect to similarity transformation η for some values of Dufour parameter Du and Schmidt number Sc

It is observed from Fig. 16 that velocity profiles decrease with the increase in Dufour parameter Du and Schmidt number Sc and thus cause thinning of the corresponding boundary layers.

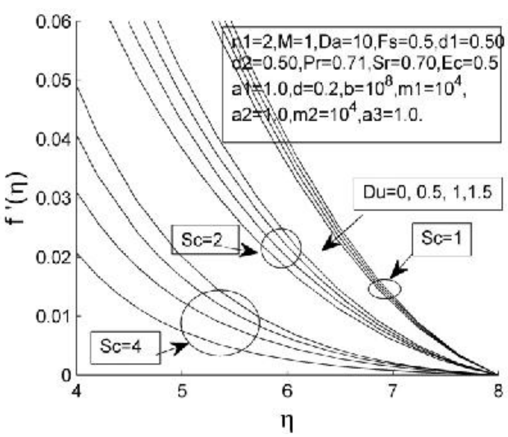

Fig. 17. Velocity profile $f'(\eta)$ with respect to similarity transformation η for some values of Dufour parameter Du and Schmidt number Sc

It is observed from Fig. 17 that velocity profiles decrease with the increase in Dufour parameter Du and Schmidt number Sc and thus cause thinning of the corresponding boundary layers.

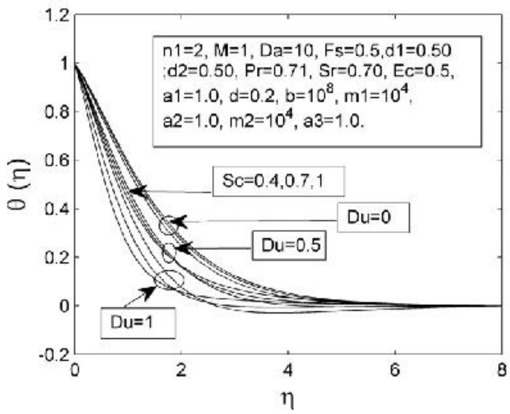

Fig. 18. Temperature profile $\theta(\eta)$ with respect to similarity transformation η for some values of Dufour parameter Du and Schmidt number Sc

It is shown in Fig. 18 that with the variation in the value of Dufour parameter Du and Schmidt number Sc, the temperature profiles show presence of point of intersection at some value of similarity variable in its (similarity variable's) range. Before the point of intersection temperature profiles decrease and after the point of intersection temperature profiles increase with the increase in Dufour parameter Du and Schmidt number Sc, and thus causes thinning before the point of intersection and thickening after the point of intersection of the corresponding boundary layers.

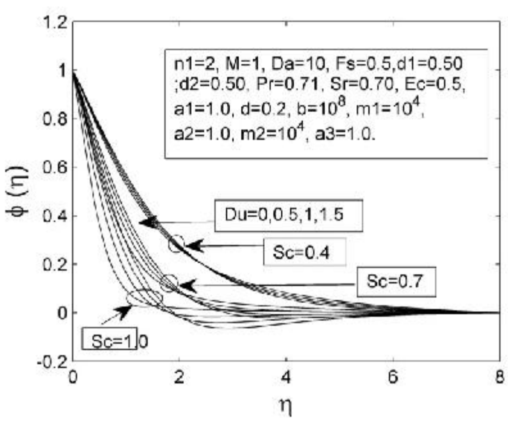

Fig. 19. Concentration profile $\phi(\eta)$ with respect to similarity transformation η for some values of Dufour parameter Du and Schmidt parameter Sc

It is shown in Fig. 19 that with the variation in the value of Dufour parameter Du and Schmidt number Sc, the concentration profiles show presence of point of intersection at some value of similarity variable in its (similarity variable's) range. Before the point of intersection concentration profiles decrease and after the point of intersection concentration profiles increase with the increase in Dufour parameter Du and Schmidt number Sc, and thus causes thinning before the point of intersection and thickening after the point of intersection of the corresponding boundary layers.

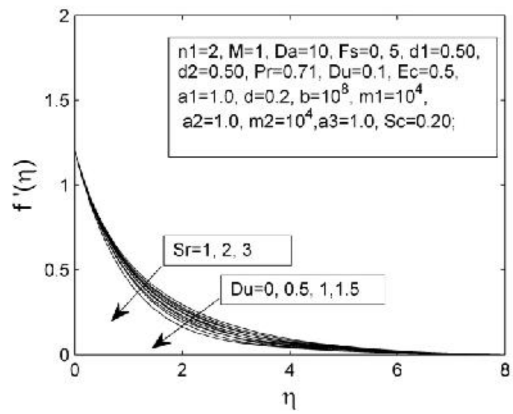

Fig. 20. Velocity profile $f'(\eta)$ with respect to similarity transformation η for some values of Dufour parameter and Soret parameter Sr

It is observed from Fig. 20 that velocity profiles decrease with the increase in Dufour parameter Du and Soret parameter Sr and thus cause thinning of the corresponding boundary layers.

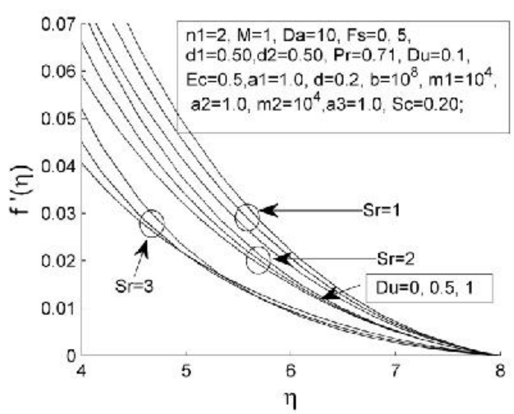

Fig. 21. Velocity profile $f'(\eta)$ with respect to similarity transformation η for some values of Dufour parameter and Soret parameter Sr

It is observed from Fig. 21 that velocity profiles decrease with the increase in Dufour parameter Du and Soret parameter Sr and thus cause thinning of the corresponding boundary layers.

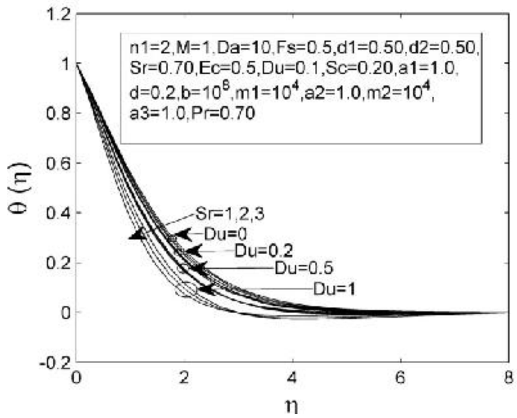

Fig. 22. Temperature profile $\theta(\eta)$ with respect to similarity transformation η for some values of Dufour parameter Du and Soret parameter Sr

It is shown in Fig. 22 that with the variation in the value of Dufour parameter Du and Soret parameter Sr, the temperature profiles show presence of point of intersection at some value of similarity variable in its (similarity variable's) range. Before the point of intersection temperature profiles decrease and after the point of intersection temperature profiles increase with the increase in Dufour parameter Du and Soret parameter Sr, and thus causes thinning before the point of intersection and thickening after the point of intersection of the corresponding boundary layers.

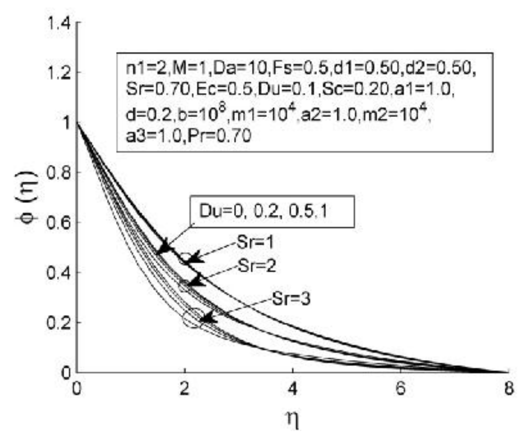

Fig. 23. Concentration profile $\phi(\eta)$ with respect to similarity transformation η for some values of Dufour parameter Du and Soret parameter Sr

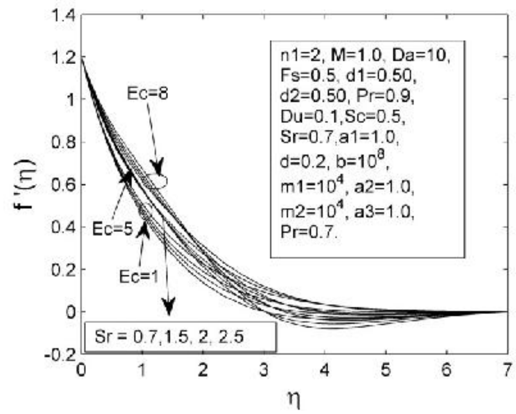

Fig. 24. Velocity profile $f'(\eta)$ with respect to similarity transformation η for some values of Soret parameter Sr and Eckelt parameter Ec

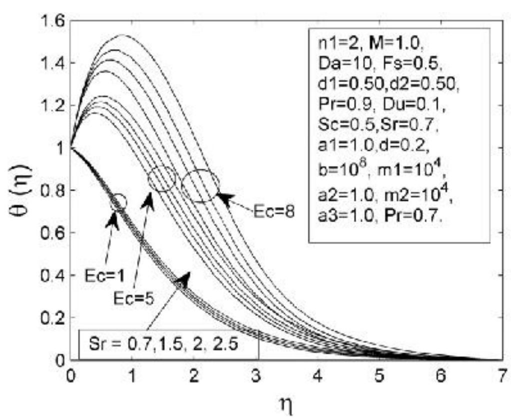

Fig. 25. Temperature profile $\theta(\eta)$ with respect to similarity transformation η for some values of Soret parameter Sr and Eckert parameter Ec

It is shown in Fig. 23 that with the variation in the value of Dufour parameter Du and Soret parameter Sr, the concentration profiles show presence of point of intersection at some value of similarity variable in its (similarity variable's) range. Before the point of intersection concentration profiles decrease and after the point of intersection concentration profiles increase with the increase in Dufour parameter Du and Soret parameter Sr, and thus causes thinning before the point of intersection and thickening after the point of intersection of the corresponding boundary layers.

It is observed from Fig. 24 that velocity profile decreases with the increase in Soret parameter Sr, thus cause thinning of the corresponding boundary layer an increases with the increase Eckert number Ec thus cause thickening of the corresponding boundary layer.

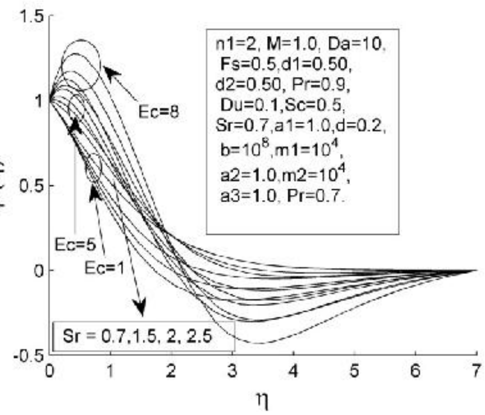

Fig. 26. Concentration profile $\phi(\eta)$ with respect to similarity transformation η for some values of Soret parameter Sr and Eckert parameter Ec

It is observed from Fig. 25 that with the variation in the value of Soret parameter Sr, and Eckert number Ec, each of the temperature profiles shows maxima and point of inflexion in the range of similarity variable. With the each value of Soret parameter Sr, and Eckert number Ec, each curve shows having maxima before the point of inflexion. Also with the increase in the value of Soret parameter and Eckert number, temperature profiles show increase and thus cause increase in the corresponding boundary layer thickness.

It is observed from Fig. 26 that with the variation in the value of Soret parameter Sr, and Eckert number Ec, each of the concentration profiles shows maxima and point of inflexion in the range of similarity variable. With each value of Soret parameter Sr, and Eckert number Ec, each curve shows having maxima before the point of inflexion. Also with the increase in the value of Soret parameter Sr and Eckert number, concentration profiles show increase before the point of inflexion and decrease after the point of inflexion, and hence cause increase before the point of inflexion and decrease after the point of inflexion in the corresponding boundary layer thickness.

Table 3 shows with the increase in Magnetic parameter Skin-friction, local Nusselt number and local Sherwood number decreases.

Table 4 shows with the increase in Casson parameter Skin-friction, local Nusselt number and local Sherwood number increases.

Table 3. Comparison of Skin-friction $f''(0)$, local Nusselt number $-\theta'(0)$, and local Sherwood number $-\phi'(0)$ for various values of Magnetic parameter M

n1=2;M=1;Da=10;Fs=0.5;d1=0.50;d2=0.50;Pr=0.71;Du=0.1;Ec=0.5;Sc=0.2;Sr=0.7; a1=1.0;d=0.2;b=10^8;m1=10^4;a2=1.0;m2=10^4;a3=1.0.			
M	$f''(0)$	$-\theta'(0)$	$-\phi'(0)$
1	-1.139886286400067	0.414856222735359	0.291371985956979
5	-1.707705031432430	0.240533363861078	0.236481214248188
10	-2.264381188870255	0.063274575662640	0.189093904953875
15	-2.724242857459311	-0.081367644844538	0.154636326522287

Table 4. Comparison of Skin-friction $f''(0)$, local Nusselt number $-\theta'(0)$, and local Sherwood number $-\phi'(0)$ for various values of Casson parameter b

n1=2;M=1;Da=10;Fs=0.5;d1=0.50;d2=0.50;Pr=0.70;Du=0.1;Ec=0.5;Sc=0.2;Sr=0.7; a1=1.0;d=0.2;b=10^8;m1=10^4;a2=1.0;m2=10^4;a3=1.0.			
b	$f''(0)$	$-\theta'(0)$	$-\phi'(0)$
0.1	-1.938133150664395	-6.295211331613203	-0.320484926788943
0.2	-1.473378060541108	-1.442823157565096	0.183465539708107
0.3	-1.324805467549381	-0.534950892963336	0.257221030686203
0.5	-1.214615842077180	-0.025337735376427	0.287249701545771

Table 5 shows with the increase in Darcy parameter Skin-friction, local Nusselt number and local Sherwood number increases.

Table 6 shows with the increase in Forchheimer parameter Skin-friction, local Nusselt number and local Sherwood number decreases.

Table 7 shows with the increase in Prandtl number Skin-friction decreases and local Nusselt number and local Sherwood number increases.

Table 8 shows with the increase in Eckert number Skin-friction increases and local Nusselt number and local Sherwood number decrease.

Table 5. Comparison of Skin-friction $f''(0)$, local Nusselt number $-\theta'(0)$, and local Sherwood number $-\phi'(0)$ for various values of Darcy parameter Da

n1=2;M=1;Da=10;Fs=0.5;d1=0.50;d2=0.50;Pr=0.71;Du=0.1;Ec=0.5;Sc=0.2;Sr=0.7; a1=1.0;d=0.2;b=10^8;m1=10^4;a2=1.0;m2=10^4;a3=1.0.			
Da	$f''(0)$	$-\theta'(0)$	$-\phi'(0)$
0.5	-1.428193623699829	0.328040454192572	0.262762395741959
1	-1.281374388721462	0.372846473212556	0.277173948582174
2	-1.203957866571336	0.395996971875209	0.284911124661897
3	-1.177501050005703	0.403819967527664	0.287573408826969

Table 6. Comparison of Skin-friction $f''(0)$, local Nusselt number $-\theta'(0)$, and local Sherwood number $-\phi'(0)$ for various values of Forchheimer parameter Fs

n1=2;M=1;Da=10;Fs=0.5;d1=0.50;d2=0.50;Pr=0.71;Du=0.1;Ec=0.5;Sc=0.2;Sr=0.7; a1=1.0;d=0.2;b=10^8;m1=10^4;a2=1.0;m2=10^4;a3=1.0.			
Fs	$f''(0)$	$-\theta'(0)$	$-\phi'(0)$
0.5	-1.139886286400067	0.414856222735359	0.291371985956979
1	-1.208612809561646	0.401628776298048	0.287495526076845
2	-1.338383349016651	0.376015619156389	0.280167649510050
3	-1.459425519349771	0.351486715493245	0.273342292473521

Table 7. Comparison of Skin-friction $f''(0)$, local Nusselt number $-\theta'(0)$, and local Sherwood number $-\phi'(0)$ for various values of Prandtl number Pr

n1=2;M=1;Da=10;Fs=0.5;d1=0.50;d2=0.50; Du=0.1;Ec=0.5;Sc=0.2;Sr=0.7; a1=1.0;d=0.2;b=10^8;m1=10^4;a2=1.0;m2=10^4;a3=1.0.			
Pr	$f''(0)$	$-\theta'(0)$	$-\phi'(0)$
0.7	-1.139171110747207	0.412286376828377	0.291199312367934
1	-1.157231825306829	0.478869265424159	0.296181869262054
2	-1.191414911346804	0.611623320537683	0.308360091315121
3	-1.209804887356637	0.679960625037383	0.315203633463110

Table 8. Comparison of Skin-friction $f''(0)$, local Nusselt number $-\theta'(0)$, and local Sherwood number $-\phi'(0)$ for various values of Eckert number Ec

n1=2;M=1;Da=10;Fs=0.5;d1=0.50;d2=0.50;Pr=0.70;Du=0.1;Ec=0.5;Sc=0.2;Sr=0.7; a1=1.0;d=0.2;b=10^8;m1=10^4;a2=1.0;m2=10^4;a3=1.0.			
Ec	$f''(0)$	$-\theta'(0)$	$-\phi'(0)$
0.1	-1.147988244422926	0.540232249116676	0.307582454320623
0.2	-1.145767434719725	0.507907740910780	0.303440467248767
0.3	-1.143558180413784	0.475809857492194	0.299329499846729
0.5	-1.139171110747207	0.412286376828377	0.291199312367934

Table 9. Comparison of Skin-friction $f''(0)$, local Nusselt number $-\theta'(0)$, and local Sherwood number $-\phi'(0)$ for various values of Dufour number Du

n1=2;M=1;Da=10;Fs=0.5;d1=0.50;d2=0.50;Pr=0.70;Du=0.1;Ec=0.5;Sc=0.2;Sr=0.7; a1=1.0;d=0.2;b=10^8;m1=10^4;a2=1.0;m2=10^4;a3=1.0.			
Du	$f''(0)$	$-\theta'(0)$	$-\phi'(0)$
0	-1.139341254219237	0.400032497066902	0.296468803292375
0.2	-1.143544759569682	0.417496237457631	0.297833579239204
0.5	-1.150011965516246	0.444375863555847	0.299947517761085
1	-1.161253400554637	0.491133315364581	0.303662254401080

Table 10. Comparison of Skin-friction $f''(0)$, local Nusselt number $-\theta'(0)$, and local Sherwood number $-\phi'(0)$ for various values of Schmidt number Sc

n1=2;M=1;Da=10;Fs=0.5;d1=0.50;d2=0.50;Pr=0.71;Du=0.1;Ec=0.5;Sc=0.2;Sr=0.7; a1=1.0;d=0.2;b=10^8;m1=10^4;a2=1.0;m2=10^4;a3=1.0.			
Sc	$f''(0)$	$-\theta'(0)$	$-\phi'(0)$
0.2	-1.139886286400067	0.414856222735359	0.291371985956979
0.4	-1.176935210977778	0.386151355496659	0.443770131850051
0.7	-1.215081398526230	0.360817373104762	0.628942510557584
1.2	-1.255405680773496	0.343770968980801	0.873476192982244

Table 11. Comparison of Skin-friction $f''(0)$, local Nusselt number $-\theta'(0)$, and local Sherwood number $-\phi'(0)$ for various values of Soret number Sr

n1=2;M=1;Da=10;Fs=0.5;d1=0.50;d2=0.50;Pr=0.70;Du=0.1;Ec=0.5;Sc=0.2;Sr=0.7; a1=1.0;d=0.2;b=10^8;m1=10^4;a2=1.0;m2=10^4;a3=1.0.			
Sr	$f''(0)$	$-\theta'(0)$	$-\phi'(0)$
0.7	-1.143632365431753	0.405620505160762	0.302985470126012
1.5	-1.154724386800227	0.397577058525297	0.340314127119831
2	-1.161673814489628	0.392217170730794	0.362464009525076
2.5	-1.168628603664313	0.386577782183745	0.383611994611814

Table 9 above shows with the increase in Dufour number, Skin-friction decreases and local Nusselt number and local Sherwood number increase.

Table 10-11 above shows with the increase in Schmidt number and Soret parameter, Skin-friction, and local Nusselt number decrease and local Sherwood number increases.

5. CONCLUSION

In the present paper the numerical study of effects of Soret and Dufour and viscous dissipation parameters on steady magnetohydrodynamic Casson fluid flow through non-Darcy porous medium is explored. By suitable similarity transformations, the governing boundary layer equations are transformed to ordinary differential equations. The method, the numerical computation with bvp4c, a MATLAB program, is applied to solve these equations. The effects of magnetic Parameter, Soret parameter, Dufour parameter, Prandtl number, Schmidt number, Eckert number, and Casson parameter on velocity, heat transfer, and concentration profiles, Skin- frictions, local Nusselt number and local Sherwood number are computed and discussed numerically and presented through tables and graphs.

From the above work following results are concluded.

Velocity profiles decrease and thus cause thinning of the corresponding boundary layers with the increase in Magnetic parameter, Dufour parameter, Soret parameter, Casson parameter, Prandtl number, and Schmidt number.

Temperature profiles decrease and thus cause thinning of the corresponding boundary layers with the increase in Dufour parameter, Casson parameter, Prandtl number, and Schmidt number.

Concentration profiles decrease and thus cause thinning of the corresponding boundary layers with the increase in Soret parameter, and Schmidt number.

Before the point of inflexion concentration profile decreases and after the point of inflexion concentration profile increases and thus causes thinning before the point of inflexion and thickening after the point of inflexion of the corresponding boundary layer, with the increase in Dufour parameter, and Casson parameter.

Velocity profiles increase and thus cause thickening of the corresponding boundary layers with the increase in Eckert number.

Temperature profiles increase and thus cause thickening of the corresponding boundary layers with the increase in magnetic parameter, Soret parameter, Eckert number.

Concentration profiles increase and thus cause thickening of the corresponding boundary layers with the increase in magnetic parameter.

Concentration profiles show increase before the point of inflexion and decrease after the point of inflexion, and hence cause increase before the point of inflexion and decrease after the point of inflexion in the corresponding boundary layer thickness, with the increase in the value of Soret parameter and Eckert number.

Skin-friction increases with the increase in Casson parameter, Darcy parameter, Prandtl number, and Dufour parameter.

Local Nusselt number increases with the increase in Casson parameter, Darcy parameter, Eckert number, Schmidt number, and Soret parameter.

Local Sherwood number increases with the increase in Casson parameter, Darcy parameter, Eckert number, Schmidt number.

Skin friction decreases with the increase in Magnetic parameter, Forchheimer parameter, Eckert number, Schmidth number, and Soret parameter.

Local Nusselt number decreases with the increase in Magnetic parameter, Forchheimer parameter, Prandtl number, and Dufour parameter.

Local Sherwood number decreases with the increase in Magnetic parameter, Forchheimer parameter, Prandtl number, Dufour parameter, Schmidth number, and Soret parameter.

COMPETING INTERESTS

Author has declared that no competing interests exist.

REFERENCES

1. Casson N. In: Mill CC, editor. A flow equation for pigment oil-suspensions of the printing ink type. Rheology of Disperse Systems, 84.Pergamon Press; 1959.
2. Bird RB, Dai GC, Yarusso BJ. The rheology and flow of viscoplastic materials. Rev Chem Eng. 1983;1:1–83.
3. Sakiadis BC, Boundary layer behavior on continuous solid surfaces: II. The boundary layer on continuous flat surface, AIChE J. 1961;7:221–225.
4. Crane LJ, Flow past a stretching plane, Angew Z. Math. Phys. 1970;21:645–647.
5. Nield DA, Bejan AA, Convection in porous media. 2nd ed. Springer, New York; 1999.
6. Mukhopadhyay Swati. Casson fluid flow and heat transfer over a nonlinearly stretching surface. Chin. Phys. B. 2013; 22(7) 074701
   DOI: 10.1088/1674-1056/22/7/074701
7. Mustafa M, Junaid Ahmad Khan. Model for flow of casson nanofluid past a non-linearly stretching sheet considering magnetic field effects. AIP Advances 5, 077148; 2015.
   Available:http://dx.doi.org/10.1063/1.4927449
8. Medikare M, Joga S, Chidem KK, MHD Stagnation point flow of a casson fluid over a nonlinearly stretching sheet with viscous dissipation. American Journal of Computational Mathematics. 2016;6:37-48.
   Available:http://dx.doi.org/10.4236/ajcm.2016.61005
9. Pramanik S. Casson fluid flow and heat transfer past an exponentially porous stretching surface in presence of thermal radiation. Ain Shams Engineering Journal. 2014;5:205–212.
   Available:http://dx.doi.org/10.1016/j.asej.2013.05.003

10. Raju CSK, Sandeep N, Sugunamma V, Jayachandra Babu M, Ramana Reddy JV. Heat and mass transfer in magnetohydrodynamic casson fluid over an exponentially permeable stretching surface. Engineering Science and Technology, an International Journal. 2016;19:45–52. Available:http://dx.doi.org/10.1016/j.jestch.2015.05.010
11. Saidulu N, Venkata Lakshmi A. Slip effects on MHD flow of casson fluid over an exponentially stretching sheet in presence of thermal radiation, heat source/sink and chemical reaction .European Journal of Advances in Engineering and Technology. 2016;3(1):47-55.
12. Sharada K, Shankar B. MHD Mixed Convection Flow of a casson fluid over an exponentially stretching surface with the effects of soret, dufour, thermal radiation and chemical reaction. World Journal of Mechanics. 2015;5:165-177. Available:http://dx.doi.org/10.4236/wjm.2015.59017
13. Swati Mukhopadhyay, Krishnendu Bhattacharyya, Tasawar Hayat. Exact solutions for the flow of Casson fluid over a stretching surface with transpiration and heat transfer effects. Chin. Phys. 2013; 22(11):114701. DOI: 10.1088/1674-1056/22/11/114701
14. Hayat T, Shehzadi SA, Alsaedi A. Soret and dufour effects on magnetohydrodynamic (MHD) flow of casson fluid. Appl Math Mech (English Ed.). 2012;33(10):1301–12.
15. Mahdy A. Heat transfer and flow of a casson fluid due to a stretching cylinder with the soret and dufour effects. Journal of Engineering Physics and Thermophysics. 2015;88(4).
16. Animasaun IL. Effects of thermophoresis, variable viscosity and thermal conductivity on free convective heat and mass transfer of non-darcian MHD dissipative Casson fluid flow with suction and nth order of chemical reaction. Journal of the Nigerian Mathematical Society. 2015;34:11–31. Available:http://dx.doi.org/10.1016/j.jnnms.2014.10.008
17. Imran Ullah, Sharidan Shafie, Ilyas Khan, Effects of slip condition and Newtonian heating on MHD flow of casson fluid over a nonlinearly stretching sheet saturated in a porous medium. Journal of King Saud University –Science. j.jksus.05.003; 2016. Available:http://dx.doi.org/10.1016
18. Cortell R, Viscous flow and heat transfer over a nonlinearly stretching sheet. Appl. Math. Comput. 2007;184:864–873.
19. Wang CY, Free convection on a vertical stretching surface. J. Appl. Math. Mech. (ZAMM). 1989;69:418–420.
20. Gorla RSR, Sidawi I, Free convection on a vertical stretching surface with suction and blowing. Appl. Sci. Res. 1994;52:247–257.
21. Khan WA, Pop I, Boundary-layer flow of a nanofluid past a stretching sheet. Int. J. Heat Mass Transf. 2010;53:2477–2483.
22. Butt AS, Tufail MN, Asif Ali. Three-dimensional flow of a magnetohydrodynamic casson fluid over an unsteady stretching sheet embedded into a porous medium. ISSN 0021-8944, Journal of Applied Mechanics and Technical Physics. 2016;57(2):283–292. c_ Pleiades Publishing, Ltd.; 2016.
23. Shehzad SA, Hayat T, Qasim M, Asghar S. Effects of mass transfer on MHD flow of casson fluid with chemical reaction and suction. Brazilian Journal of Chemical Engineering. 2013;30(01):187-195.
24. Arthur EM, Seini IY. Bortteir LB. Analysis of casson fluid flow over a vertical porous surface with chemical reaction in the presence of magnetic field. Journal of Applied Mathematics and Physics. 2015;3: 713-723. Available:http://dx.doi.org/10.4236/jamp.2015.36085
25. Hussanan Abid, Mohd Zuki Salleh, Razman Mat Tahar, Ilyas Khan. Unsteady boundary layer flow and heat transfer of a casson fluid past an oscillating vertical plate with newtonian heating. Plos One. 2014;9(10).
26. Kirubhashankar CK, Ganesh S, Mohamed A Ismail. Casson fluid flow and heat transfer over an unsteady porous stretching surface. Applied mathematical Sciences. 2015;9(7):345–351. Available:http://dx.doi.org/10.12988/ams.2015.411988
27. Motahar Reza, Rajni Chahal, Neha Sharma. Radiation effect on MHD casson fluid flow over a power-law stretching sheet with chemical reaction. World Academy of Science, Engineering and Technology. International Journal of Chemical, Molecular, Nuclear, Materials and Metallurgical Engineering. 2016;10(5).

28. Siddiqui AM, Farooq AA, Rana MA. A Mathematical model for the flow of a casson fluid due to metachronal beating of cilia in a tube. Hindawi Publishing Corporation e Scientific World Journal. 2015;12.
Article ID 487819.
Available:http://dx.doi.org/10.1155/2015/487819
29. Shaw Sachin, Ganeswar Mahanta, Precious Sibanda. Non-linear thermal convection in a casson fluid flow over a horizontal plate with convective boundary condition. Alexandria Engineering Journal. 2016;55:1295–1304.
Available:http://dx.doi.org/10.1016/j.aej.2016.04.020
30. Rao AS, Prasad VR, Reddy NB, B´eg OA, Heat transfer in a casson rheological fluid from a semi-infinite vertical plate with partial slip, heat trans Asian Res; Published online in Wiley Online Library; 2013.
Available:wileyonlinelibrary.com/journal/htj
Available:http://dx.doi.org/10.1002/htj.21115
31. Forchheimer PZ. Wasserbewegung Durch Boden. Zeit Ver Deutsch Ing. 1901; 45:1781–8.
32. Darcy H. Les fontainer publigues de la ville de Dijoin. Dalmont; 1856.
33. Gangadhar K, Bhaskar N Reddy. chemically reacting MHD boundary layer flow of heat and mass transfer over a moving vertical plate in a porous medium with suction. Journal of Applied Fluid Mechanics. 2013;6(1):107-114.
34. Gangadhar K, Soret and dufour effects on hydro magnetic heat and mass transfer over a vertical plate with a convective surface boundary condition and chemical reaction Journal of Applied Fluid Mechanics. 2013;6(1):95-105.
35. Gangadhar K, Radiation heat generation and viscous dissipation effects on MHD boundary layer flow for the blasius and sakiadis flows with a convective surface boundary condition. Journal of Applied Fluid Mechanics. 2015;8(3):559-570.
36. Mohammed Ibrahim S, Gangadhar K, Bhaskar N Reddy. Radiation and mass transfer effects on MHD oscillatory flow in a channel filled with porous medium in the presence of chemical reaction. Journal of Applied Fluid Mechanics. 2015;8(3):529-537.
37. Srinivasa Raju R, Jithender Reddy G, Anand Rao J, Rashidi MM, Rama Subba Reddy Gorla. Analytical and numerical study of unsteady MHD free convection flow over an exponentially moving vertical plate with heat absorption. International Journal of Thermal Sciences. 2016;107: 303–315.
38. Srinivasa Raju R, Jitthender Reddy G, Anand Rao J, Rashidi MM, Thermal diffusion and diffusion thermo effects on an unsteady heat and mass transfer MHD natural convection couette flow using FEM. Journal of Computational Design and Engineering. 2016;3(4):349–362.
DOI: 10.1016/j.jcde.2016.06.003
39. Srinivasa Raju R, Effects of soret and dufour on natural convective fluid flow past a vertical plate embedded in porous medium in presence of thermal radiation via FEM. Journal of the Korean Society for Industrial and Applied Mathematics. 2016;20(4):309–332.
40. Srinivasa Raju R, Anil Kumar M, Dharmendar Reddy Y. Unsteady MHD free convective flow past a vertical porous plate with variable suction. ARPN Journal of Engineering and Applied Sciences. 2016;11(23):13608–13616.
41. Srinivasa Raju R, Venkatesh N, Anil Kumar M, Jithender Reddy G. Influence of transpiration on unsteady heat transfer mhd fluid flow over an infinite vertical plate in presence of hall current. ARPN Journal of Engineering and Applied Sciences. 2016;11(23):14008–14013.
42. Jitthender Reddy G, Srinivasa Raju R, Anand Rao J. Thermal diffusion and diffusion thermo impact on chemical reacted MHD free convection from an impulsively started infinite vertical plate embedded in a porous medium using FEM. Journal of Porous Media; 2016 (In press).
43. Ramya Dodda R. Srinivasa Raju J. Anand Rao. Numerical simulation of MHD boundary layer partial slip flow of nanofluids over a nonlinear stretching sheet with suction/injection. Journal of Nanofluids; 2016 (In press).
44. Sailaja SV, Shanker B, Srinivasa Raju R, Double diffusive effects on MHD mixed convection Casson fluid flow towards a vertically inclined plate filled in porous medium in presence of Biot number: A finite element technique. Journal of Nanofluids; 2016 (In press).

45. Jitthender Reddy G, Srinivasa Raju R, Anand Rao J, Rama Subba Reddy Gorla, Unsteady MHD Couette flow of water at 4°C in a rotating system in presence of heat transfer with ramped temperature via finite element method. International Journal of Applied Mechanics and Engineering; 2016 (In press).
46. Srinivasa Raju R. Influence of angle of inclination on unsteady MHD Casson fluid flow past a vertical surface filled by porous medium in presence of constant heat flux, chemical reaction and viscous dissipation. Journal of Nanofluids; 2016 (In press).
47. Ramachandra Prasad V, Subba Rao A, Bhaskar Reddy N, Vasu B, Anwar Be´g O, Modelling laminar transport phenomena in a Casson rheological fluid from a horizontal circular cylinder with partial slip, Proc IMechE- Part E: J. Process Mechanical Engineering. 2013;227(4):309-326.
48. Subba Rao A, Ramachandra Prasad V, Nagendra N, Bhaskar Reddy N, Anwar Beg O. Non-similar computational solution for boundary layer flows of non-newtonian fluid from an inclined plate with thermal slip. Journal of Applied Fluid Mechanics. 2016;9(2)795-807.
ISSN 1735-3572
EISSN 1735-3645
Available:www.jafmonline.net
49. Md Jashim Uddin, Md Yusoff NH, Anwar Be´g O, Ahamd Izani Ismail. Lie group analysis and numerical solutions for non-Newtonian nanofluid flow in a porous medium with internal heat generation, IOP Publishing Physica Scripta, 2013; 87(02540)1:14.
DOI: 10.1088/0031-8949/87/02/025401
50. Anwar Bég O, Bakier AY, Prasad VR. Numerical study of free convection magnetohydrodynamic heat and mass transfer from a stretching surface to a saturated porous medium with Soret and Dufour effects, Computational Materials Science. 2009;46(1):57-65.
51. Beg A, Ferdows M, Beg ETA, Ahmed, T, Wahiduzzaman M, Alam MM, Numerical investigation of radiative optically-dense transient magnetized reactive transport phenomena with cross diffusion, dissipation and wall mass flux effects. Journal of the Taiwan Institute of Chemical Engineers, J. Taiwan Inst. Chemical Engineers. 2016;15.
DOI: ORG/10.1016/J.JTICE.2016.06.003
52. Akbar NS, Tripathi D, Beg A, Khan ZH, MHD dissipative flow and heat transfer of casson fluids due to metachronal wave propulsion of beating cilia with thermal and velocity slip effects under an oblique magnetic field. Acta Astronautica. 2016; 128:1-12.
53. Ali N, Ullah Khan S, Abbas Z, Hydromagnetic flow and heat transfer of a jeffrey fluid over an oscillatory stretching surface. Zeitschrift für Naturforschung A. 2015;70(7)a: 567–576.
54. SU Khan, N Ali, Z Abbas, Hydromagnetic flow and heat transfer over a porous oscillating stretching surface in a viscoelastic fluid with porous medium, Plos One. 2015;10(12):e0144299.
55. N Ali, SU Khan, Z Abbas, Unsteady flow of third grade fluid over an oscillatory stretching sheet with thermal radiation and heat source/sink. Nonlinear Engineering. 2015;4(4):223–236.
56. Ali N, SU Khan, Z Abbas, Sajid M. Soret and Dufour effects on hydromagnetic flow of viscoelastic fluid over porous oscillatory stretching sheet with thermal radiation. Journal of the Brazilian Society of Mechanical Sciences and Engineering. 2016;38:2533-2546.
57. Ali N, Khan SU, Sajid M, Abbas Z. MHD flow and heat transfer of couple stress fluid over an oscillatory stretching sheet with heat source/sink in porous medium. Alexandria Engineering Journal. 2016;55: 915–924.
58. Nasir A, Khan SU, Sajid M, Abbas Z. Flow and heat transfer of hydromagnetic Oldroyd-B fluid in a channel with stretching walls. Nonlinear Engineering. 2016;5(2): 73–79.

Peer-review history:
The peer review history for this paper can be accessed here:
http://prh.sdiarticle3.com/review-history/ 17761